Mechanism for phase separation in cuprates and related multiband systems

A. O. Sboychakov,[1,2] Sergey Savel'ev,[1,3] A. L. Rakhmanov,[1,2,3] K. I. Kugel,[2,3] and Franco Nori[1,4]
[1]*Advanced Science Institute, The Institute of Physical and Chemical Research (RIKEN), Wako-shi, Saitama, 351-0198, Japan*
[2]*Institute for Theoretical and Applied Electrodynamics of Russian Academy of Sciences, Izhorskaya Str. 13, 125412 Moscow, Russia*
[3]*Department of Physics, Loughborough University, Loughborough LE11 3TU, United Kingdom*
[4]*Center for Theoretical Physics, CSCS, Department of Physics, University of Michigan, Ann Arbor, Michigan 48109-1040, USA*
(Received 26 March 2008; revised manuscript received 16 May 2008; published 11 June 2008)

A two-band Hubbard model in the limit of strong on-site Coulomb repulsion is used to describe the band structure and phase separation (PS) in strongly correlated electron systems with a special emphasis on cuprate superconductors. The PS corresponding to the inhomogeneous charge density occurs in such a system due to the redistribution of charge carriers between the bands. This mechanism does not require any magnetic interaction or intersite Coulomb repulsion. The interband hybridization gives rise to a peak in the electron density of states and, in the PS state, the Fermi level in one of the phase is located near this peak. The resulting charge density redistribution can affect the dependence of the superconducting critical temperature T_c on the doping level.

DOI: 10.1103/PhysRevB.77.224504 PACS number(s): 74.72.−h, 71.27.+a, 74.20.−z, 74.25.Dw

I. INTRODUCTION

The phenomenon of self-organized electron inhomogeneity or phase separation (PS) is common to many strongly correlated electron systems.[1,2] For example, PS in the form of droplets, stripes, and checkerboard patterns has been observed in doped magnetic oxides (manganites).[1] Nanoscale spatial variations in the electronic characteristics are also observed in different high-T_c superconductors in the form of stripes,[1] granular droplet-like structures,[3] four-unit-cell periodic (checkerboard) patterns,[4] or even more intricate arrangements.[5] Such inhomogeneous electron structures in superconducting cuprates and related materials are predicted by several theoretical models.[6–13]

The important role of PS for superconductivity in cuprates was widely discussed starting from the late 1980s. The cuprates are an example of strongly correlated electron systems usually studied in the framework of the multiband Hubbard model and its generalizations.[12,14–23] Many theoretical approaches (see, e.g., Refs. 1, 2, and 7–11) explain PS in manganites and cuprates as a result of the competition between electron localization due to antiferromagnetic correlations and delocalization in the nonmagnetic (or ferromagnetic) regions. It should be noted, however, that the phase separation is observed in cuprates in a wide doping range, even near optimal doping, where one could not expect significant antiferromagnetic correlations.[24–26] Another possibility that was discussed in the literature is the formation of inhomogeneous structures due to the nearest-neighbor Coulomb repulsion.[12,15–20] In both cases, the existence of spin or charge degrees of freedom is essential for PS, whereas specific features of the band structure do not play a fundamental role. Even when the multiband Hubbard Hamiltonian is reduced to the effective single-band model, PS can arise.[20] However, as it was predicted in Ref. 27 based on the mean-field (Hubbard I) approximation, PS can arise in two-band (or multiband) Hubbard models due to the on-site Coulomb repulsion in the absence of any fluctuations related to a magnetic or charge order. This mechanism of PS is based on the following physical idea: the strong Coulomb correlations make the width of one band dependent on the occupation of another band. When the Fermi level is in the region where the two bands overlap, the redistribution of the charge carriers between the bands gives rise to a nonmonotonic dependence of the energy on the doping level. In certain range of parameters (e.g., when the hopping integrals for the two bands are significantly different), the energy as a function of the doping can have two minima. So, it may be favorable for the system to form an inhomogeneous state consisting of two phases with the charge carrier densities corresponding to these minima. Here we apply the approach of Ref. 27 to the analysis of the PS, taking into account interband hybridization, which is an important feature of the cuprates.[22] Analyzing the Hubbard model in the Hubbard I approximation, we show that the multiband (in particular, two-band) nature of the cuprates gives rise to PS in a wide range of the model parameters *without* antiferromagnetic correlations or any additional terms (e.g., nearest-neighbor Coulomb interaction) in the usual Hubbard Hamiltonian.

The two-band Hubbard model allows us to describe the PS of the droplet-type (including the droplet size) observed in experiments (see, e.g., Refs. 3 and 5). This mechanism for PS produces a density of states (DOS) at the Fermi level, which corresponds to the optimum doping in one of the phases. As a result of the PS, the number of charge carriers in the system is not directly determined by the doping level and can depend on temperature. The difference between the doping level and the number of charge carriers occurs, in particular, for superconducting cuprates.[22,26,28,29] It is possible that a slow variation of the critical temperature observed within a broad doping range in high-T_c superconductors is related to such type of PS.

II. TWO-BAND HUBBARD MODEL

Many theoretical studies of the electronic properties of the superconducting cuprates are based on the multiband Hubbard Hamiltonian accounting the hybridization of oxygen p

orbitals with copper d orbitals.[22] The commonly used model to describe superconducting cuprates is based on the Hubbard Hamiltonian with three bands: Cu($3d_{x^2-y^2}$), O($2p_x$), and O($2p_y$).[22] In earlier studies, this Hamiltonian was reduced to an effective single-band Hubbard Hamiltonian.[16,20,22,30] However, recent computations (see, e.g., Refs. 31 and 32) show that two distinguishable Cu-O bond lengths in the CuO_6 octahedron and the direct tunneling of holes between the oxygen atoms lead to the effective two-band Hubbard Hamiltonian:[32]

$$\mathcal{H} = -\sum_{\langle \mathbf{nm}\rangle \alpha\beta\sigma} t^{\alpha\beta}(a^{\dagger}_{\mathbf{n}\alpha\sigma}a_{\mathbf{m}\beta\sigma} + \text{H.c.}) - \sum_{\mathbf{n}\alpha\sigma}(\mu + \epsilon_{\alpha})n_{\mathbf{n}\alpha\sigma} + \frac{1}{2}\sum_{\mathbf{n}\alpha,\sigma} U^{\alpha} n_{\mathbf{n}\alpha\sigma}n_{\mathbf{n}\alpha\bar{\sigma}} + \frac{U'}{2}\sum_{\mathbf{n}\alpha,\sigma\sigma'} n_{\mathbf{n}\alpha\sigma}n_{\mathbf{n}\bar{\alpha}\sigma'}. \quad (1)$$

Here, $a^{\dagger}_{\mathbf{n}\alpha\sigma}$ and $a_{\mathbf{n}\alpha\sigma}$ are the creation and annihilation operators for holes in the state $\alpha=\{p,d\}$ at site $\mathbf{n}$ with spin projection σ ($\bar{\alpha},\bar{\sigma}$ denote not-α and not-σ), the symbol $\langle\ldots\rangle$ denotes a summation over the nearest sites, μ is the chemical potential, ϵ_d is the energy difference between the centers of the d and p bands, and $\epsilon_p=0$. The first term in Eq. (1) is the kinetic energy of the conduction holes; the second term is due to the chemical potential and the shift between the centers of d and p bands. The last two terms correspond, respectively, to the intraband and interband on-site Coulomb repulsion. In agreement to Ref. 32, we assume that the Coulomb interaction is strong enough, that is U^{α}, $U' \gg t^{\alpha\beta}$, ϵ_d. Applying the Hubbard I approximation, $\langle \hat{T}a_{\mathbf{m}\alpha\sigma}(t)n_{\mathbf{n}\beta\sigma'}(t)a^{\dagger}_{\mathbf{n}_0\alpha\sigma}(t_0)\rangle \to \langle n_{\mathbf{n}\beta\sigma'}\rangle\langle \hat{T}a_{\mathbf{m}\alpha\sigma}(t)a^{\dagger}_{\mathbf{n}_0\alpha\sigma}(t_0)\rangle$ ($\hat{T}$ is time-ordering operator), for Hamiltonian (1), we derive the relationship

$$(\omega + \mu + \epsilon^{\alpha})G_{\alpha\beta}(\omega,\mathbf{k}) = g_{\alpha}\left(1 + \sum_{\gamma}\varepsilon^{\alpha\gamma}(\mathbf{k})G_{\gamma\beta}(\omega,\mathbf{k})\right), \quad (2)$$

for the one-particle Green's functions $G_{\alpha\beta,\sigma\sigma'}(\mathbf{n}-\mathbf{n}_0,\ t-t_0) = -i\langle \hat{T}a_{\mathbf{n}\alpha\sigma}(t)a^{\dagger}_{\mathbf{n}_0\beta\sigma'}(t_0)\rangle$ in the frequency-momentum $(\omega,\mathbf{k})$ representation, where $g_{\alpha}=1-n_{\bar{\alpha}}-n_{\alpha}/2$. The form of the function $\varepsilon^{\alpha\beta}(\mathbf{k})$ depends on the symmetry of the crystal lattice. We analyze here a simple cubic lattice. In this case, $\varepsilon^{\alpha\beta}(\mathbf{k})=w^{\alpha\beta}\zeta(\mathbf{k})$, $w^{\alpha\beta}=zt^{\alpha\beta}$, and $\zeta(\mathbf{k})=-[\cos(k_1d)+\cos(k_2d)+\cos(k_3d)]/3$, where d is the lattice constant. Below we consider a purely paramagnetic state, that is, $n_{\alpha\uparrow}=n_{\alpha\downarrow}=n_{\alpha}/2$, and neglect the $\langle a^{\dagger}_{\alpha}a_{\bar{\alpha}}\rangle$ averages. Note, however, that the latter assumption does not significantly affect the results obtained.[33]

The Hubbard I approximation is an appropriate method to find the main features of the electron band structure, which is confirmed by comparison to experiments and numerical results.[34] It is well known that the Hubbard I approximation overestimates the electron-electron correlations. In particular, it leads to an energy gap even at small values of U. The main problems with the Hubbard model arise when $t\sim U$ and the situation in this parameter range is still under discussion even for more advanced approximations than Hubbard I. Nevertheless, when $t \ll U$ the situation is relatively simpler, and the Hubbard I approximation captures the main correlation effect, that is, the dependence of the band width on the number of charge carriers (see, e.g., Ref. 35). The other correlation effects are related to nonzero spin correlation functions and finite U, which we do not consider here, limiting ourselves to the case $U\to\infty$.

Equation (2) forms a linear set of equations for $G_{\alpha\beta}$, which can be easily solved. The calculated Green's functions determine the DOS and the energy of the system. Following this approach, we derive the DOS,

$$\rho_{\alpha\beta}(E) = -\frac{1}{\pi}\int \frac{d^3\mathbf{k}}{(2\pi)^3}\text{Im}\,[G_{\alpha\beta}(\omega + i0,\mathbf{k})]\big|_{\omega+\mu=E}, \quad (3)$$

in the form

$$\rho_{\alpha\beta}(E) = \sqrt{g_{\alpha}g_{\beta}}\sum_{j=\pm1}\int \frac{d^3\mathbf{k}}{(2\pi)^3}v^j_{\alpha}(\mathbf{k})v^j_{\beta}(\mathbf{k})\,\delta(E-\bar{\varepsilon}_j(\mathbf{k})), \quad (4)$$

where $\bar{\varepsilon}_j[\zeta(\mathbf{k})]$ and $v^j_{\alpha}[\zeta(\mathbf{k})]$ are the eigenvalues and eigenvectors of the matrix $\bar{\varepsilon}^{\alpha\beta}(\zeta)=\sqrt{g_{\alpha}g_{\beta}}w^{\alpha\beta}\zeta-\delta_{\alpha\beta}\epsilon^{\alpha}$. Solving this eigenvalue problem, we obtain the energy spectrum $\bar{\varepsilon}_j(\mathbf{k})$ of charge carriers in two new bands (labeled by $j=\pm1$) and coefficients v^j_{α}, determining the transformation from p and d holes to the quasiparticles in these bands

$$\bar{\varepsilon}_j(\zeta(\mathbf{k})) = \frac{1}{2}\{(\bar{w}^{aa}+\bar{w}^{bb})\zeta - \epsilon - j\sqrt{[(\bar{w}^{aa}-\bar{w}^{bb})\zeta+\epsilon]^2 + 4(\bar{w}^{ab})^2}\}, \quad (5)$$

$$v^j(\zeta) = \frac{1}{\sqrt{[\bar{w}^{aa}\zeta-\bar{\varepsilon}_j]^2 + (\bar{w}^{ab})^2\zeta^2}}\begin{pmatrix} -\bar{w}^{ab}\zeta \\ \bar{w}^{aa}\zeta - \bar{\varepsilon}_j, \end{pmatrix}, \quad (6)$$

where $\bar{w}^{\alpha\beta}=\sqrt{g_{\alpha}g_{\beta}}w^{\alpha\beta}$. In contrast to p and d holes with short lifetime due to interband transitions, the new quasiparticles with spectrum (5) have a longer lifetime and are scattered by, e.g., phonons and impurities. We denote the lower band as $j=1$ and the upper one as $j=-1$. We can write $\rho_{\alpha\beta}$ using the dimensionless DOS $\rho_0(E')=\int\delta[E'-\zeta(\mathbf{k})]d^3\mathbf{k}/(2\pi)^3$ of uncorrelated electrons,

$$\rho_{\alpha\beta}(E) = \sqrt{g_{\alpha}g_{\beta}}\sum_{j=\pm1} v^j_{\alpha}(\zeta)v^j_{\beta}(\zeta)\left|\frac{\partial\varepsilon_j}{\partial\zeta}\right|^{-1}\rho_0(\zeta)|_{\zeta=\bar{\zeta}_j(E)}, \quad (7)$$

where $\bar{\zeta}_j(E)$ is the inverse function of $\bar{\varepsilon}_j(E)$. The number of electrons in the state α is

$$n_{\alpha} = 2\int_{\mu_{\min}}^{\mu} dE\rho_{\alpha\alpha}(E,n_a,n_b), \quad (8)$$

where $\mu_{\min}=\bar{\varepsilon}_1(\zeta=-1)$ (note that $\rho_{\alpha\beta}$ depends on n_{α} through the functions g_{α}). The total number of charge carriers per site is $n=\Sigma_{\alpha}n_{\alpha}(\mu)$. This equality, alongside with Eqs. (5)–(8), form a set of equations for the calculation of n_{α} and μ. Employing coefficients (6), we can find the Green's functions corresponding to the band spectrum (5) and the DOS, ρ_j for two j-bands

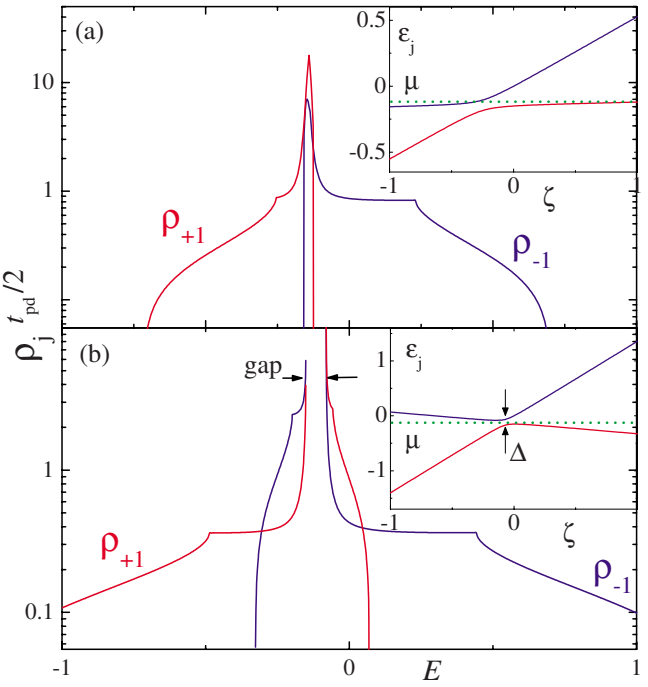

FIG. 1. (Color online) Density of states $\rho_{\pm 1}$ versus energy E for quasiparticles (holes) located in bands $j=\pm 1$ for two different types of spectra, shown in the corresponding insets. The gapless spectrum shown in the inset (a) was calculated at $n=0.6$, $\varepsilon_d=0.15$ eV, $w_{pp}=1$ eV, $w_{dd}=0.1$ eV, and relatively small interband hybridization $w_{pd}=0.25$ eV. The gapped spectrum in the inset (b) was calculated for the same parameters but for stronger interband hybridization $w_{pd}=1$ eV. In case (b), the transition to the insulating state occurs at a certain doping level for which the chemical potential μ (shown by the green dotted line) is located inside the gap. In both cases, a large peak in the DOS is observed at energies corresponding to the anticrossing of the bands, where a significant flattening of the Fermi surface (see insets) takes place. The quasiparticle energy spectra are shown in the insets as a function of the variable ζ, since ε_j depends on the crystal momentum $\mathbf{k}$ only through $\zeta(\mathbf{k})$.

$$\rho_j(E) = \left[\sum_\alpha g_\alpha [v_\alpha^j(\zeta)]^2\right] \left|\frac{\partial \varepsilon_j(\zeta)}{\partial \zeta}\right|^{-1} \rho_0(\zeta)|_{\zeta=\bar{\zeta}_j(E)}. \quad (9)$$

Each band is split into two Hubbard subbands due to the on-site Coulomb repulsion. Thus, in the two-band Hubbard model we have four bands, two lower and two upper bands, separated by a gap of the order of U. We consider here the doping range $n<1$ and in the limit $U\to\infty$, the upper Hubbard bands do not contribute to the total electron energy.

III. BAND STRUCTURE AND DENSITY OF STATES

Superconducting cuprates vary from strongly anisotropic to nearly isotropic materials. To account for this, we consider two limiting cases: square and cubic lattices. The obtained results are quite similar, and below we present the band structure and DOS (Figs. 1 and 2) calculated using Eqs. (5) and (9) only for the case of simple cubic lattice. Two qualitatively different quasiparticle spectra are shown in the insets

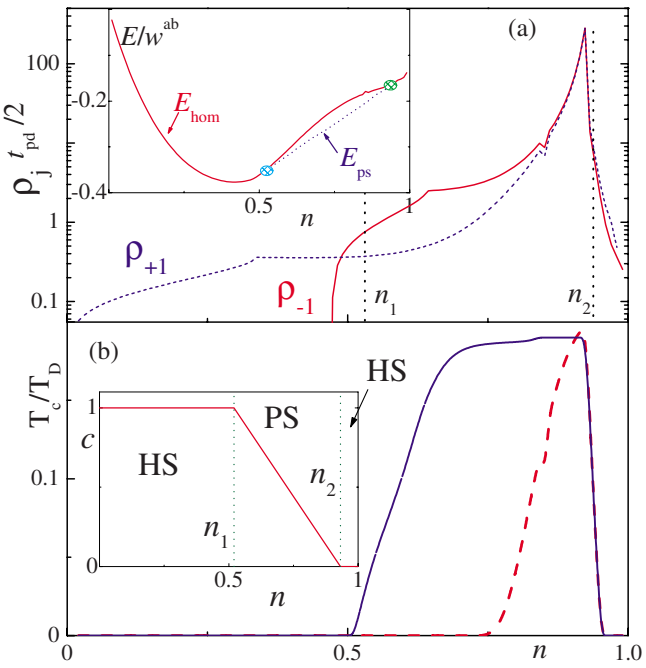

FIG. 2. (Color online) (a) The density of states at the Fermi level versus doping in the two-band Hubbard model. Inset in (a): energy of the homogeneous (red solid line) and the phase separated (blue dashed line) states. The dependence of the energy in the homogeneous state, $E_{\rm hom}$, on n has a negative curvature if $n_1<n<n_2$. In this range of doping, the PS state becomes more favorable since its energy, $E_{\rm ps}$, is lower than $E_{\rm hom}$ [see inset in (a)]. The values $n_{1,2}$ are indicated in the main panel of (a) by black vertical dotted lines. The point n_2 is near the peak in the DOS. (b) The critical temperature, T_c, of the superconducting transition versus doping level n for the homogeneous (red dashed line) and PS (blue solid line) states calculated using Eq. (12). The $T_c(n)$ of the homogeneous state decreases fast when the doping n deviates from its optimum value about n_2. In contrast to this, $T_c(n)$ in the PS state is a broad function and exhibits a plateau within the $n_1<n<n_2$ range. The inset in (b) demonstrates the dependence of the concentration c of the phase with lower hole content on n. The regions of homogeneous (HS) and PS states are indicated in the inset. Here we use the following parameters: $\varepsilon_d=0.2$ eV, $w_{pp}=1$ eV, $w_{dd}=0.3$ eV, and $w_{pd}=0.7$ eV.

of Figs. 1(a) and 1(b). The anticrossing of two bands shown in the inset in Fig. 1(a) corresponds to a metallic behavior for any doping. When doping increases, the chemical potential μ (shown by the dotted green line) shifts upward: at low doping we have one "metallic" band and one empty band; then two metallic bands; by further increasing the doping, one metallic and one filled band. For larger interband hybridization, $t^{pd}>(t^{pp}t^{dd})^{1/2}$, we obtain a transition to an insulator at some doping level. Indeed, for some doping, μ is located in the gap between zones. Nearby the anticrossing point of the two bands, the spectrum $\varepsilon_j[\zeta(\mathbf{k})]$ becomes flatter. For energies close to the anticrossing points, the DOS exhibits peaks (Fig. 1), which are large,

$$\rho_j \propto (E_0 - E)^{-1/2},$$

when n is close to 1 in the vicinity of the band gap [Fig. 1(b)]. The optimal doping for superconductivity corresponds

to the case when μ is close to the energy where the peak of the DOS is observed.

We do *not* claim to provide a detailed description of the actual energy band structure of the cuprates. For our analysis, it is of interest the existence of the peaks in the DOS near the Fermi level. In the simple model under study, the nature of these peaks is not related to some particular approximation. The peaks arise near the crossing of the initial (not renormalized) bands as it always occurs when the degeneracy of the initial bands is lifted. Note that for the two-band Hubbard model, the Fermi level could be pinned at the DOS peak related to the van Hove singularity.[36]

IV. PHASE SEPARATION

The energy,

$$E_{\mathrm{hom}}(n) = 2\sum_{j} \int_{\mu_{\min}}^{\mu} dE\, E\rho_j(E), \tag{10}$$

of the homogeneous state, versus doping n, is shown in the inset of Fig. 2(a). The curvature of $E_{\mathrm{hom}}(n)$ is negative between the two marked points n_1 and n_2. This indicates the instability of the homogeneous state with respect to the separation into two phases with hole densities n_1 and n_2, $n_1 < n < n_2$ (see, e.g., Ref. 23). The energy

$$E_{\mathrm{ps}}(n) = cE_{\mathrm{hom}}(n_1) + (1-c)E_{\mathrm{hom}}(n_2) \tag{11}$$

of the PS state with relative phase fractions c and $1-c$, which are determined by the charge conservation condition $n=cn_1+(1-c)n_2$, is lower than $E_{\mathrm{hom}}(n)$ between n_1 and n_2 [see dashed line in the inset of Fig. 2(a)]. In a wide parameter range, the hole concentration n_2 turns out to be near the optimum value. A typical dependence of the phase concentration c versus doping is shown in the inset of Fig. 2(b). For low doping, the system is in a homogeneous state ($c=1$). If $n>n_1$, the sample becomes segregated into droplets with two different hole concentrations, n_1 and n_2. Further increasing n, the relative concentration c of the phase with lower hole content n_1 decreases almost linearly, and when $n>n_2$ this phase disappears and the system becomes homogeneous again. Further analysis shows that the PS state occurs in the parameter range where $w_{pd}<w_{pp}$. If $w_{pd}\gg w_{pp}$, the two-band Hubbard Hamiltonian reduces to an effective single-band model, and the discussed cause for the PS in the system disappears. Note once more that the PS in the effective single-band models[20–22] can arise either due to nearest-neighbor Coulomb repulsion or antiferromagnetic correlations.

The PS leads to a redistribution of the charge carriers and charge neutrality breaking. The structure of the PS state can be either ordered (e.g., checkerboard structure) or random (i.e., randomly distributed droplets of one phase within a matrix of the other phase). The charge redistribution and finite droplet size give rise to the additional size-dependent terms in Eq. (11). For the random PS state, the droplet size D is determined by the competition between the Coulomb and surface energies. Following the approach developed in Ref. 23, we can estimate D in the range from three to six lattice constants d when $w_{pd}\sim w_{pp}\sim 1$ eV, in agreement with the experimental data reported in Ref. 3, where spatial variations of the DOS and superconducting gap were measured using STM.

The above results were obtained for the simple cubic lattice, which is not the actual crystal structure of high-T_c materials. However, as it was mentioned above, the rough *qualitative* picture of the PS is nearly the same for the cubic and square lattices. So the specific crystal structure is not of fundamental importance for our qualitative study of PS using the Hubbard I approximation.

V. CRITICAL TEMPERATURE VERSUS DOPING

In this section, we analyze the possible effect of the PS considered above on the critical temperature T_c of the superconducting transition. We do not focus on any particular mechanism of superconductivity in the cuprates. We just try to qualitatively relate the DOS to T_c. We also assume that T_c grows with the DOS. Then, to illustrate the possible effects, we use the simplest BCS formula for T_c, accounting for the Coulomb repulsion[38]

$$T_c = T_D \exp[-1/(\rho_j V_p - \nu_c)], \tag{12}$$

where T_D is the Debye temperature, V_p is the BCS electron-phonon coupling constant,

$$\nu_c = \rho_j V_c / [1 + \rho_j V_c \ln(\mu/k_B T_D)] \tag{13}$$

is the Coulomb pseudopotential, and $V_c\sim U^p\approx 5$ eV are the Coulomb matrix elements. Note that the possible applicability of Eq. (12) in the case of high-T_c cuprates is discussed in Ref. 29. Here, the BCS formula is only used for illustration purpose, just as an oversimplified illustration.

In our approach, the homogeneous superconducting state can appear in different bands depending on doping (see Fig. 1): in band $j=1$ for low doping and in $j=-1$ for higher doping. The dependence of T_c on doping n for the homogeneous state is shown by the dashed line in Fig. 2(b). For the chosen range of parameters, T_c is nonzero only for a narrow doping level and achieves a maximum at the optimum doping (see insets in Fig. 1). Away from the optimal doping, $T_c(n)$ decreases fast with n. In the PS state, one of the phases retains the optimum hole concentration within a wide interval of doping levels. This results in a slower decrease [see blue solid line in Fig. 2(b)] of T_c when n deviates from the optimal value n_2. This provides a possible explanation of the observed dependence of T_c on hole doping in cuprates (see Refs. 26 and 29, and references therein). Note that the above picture is related to the variation of the density of states with doping, which was widely discussed for many other models (see, e.g., Refs. 21 and 39).

VI. CONCLUSIONS

We used the two-band Hubbard model to study the mechanism of phase separation in strongly correlated electron systems without magnetic ordering, of interest for superconducting cuprates and other multiband systems with strongly correlated electrons. Using a Green's functions tech-

nique, we calculated the band structure and the density of states at the Fermi level. The density of states exhibits a large peak at the crossing of the initial energy bands. For a certain range of the model parameters, a spatial phase separation of the charge carriers occurs due to the electron redistribution between the two bands. Our estimates of the spatial scale of PS are in good agreement with important experimental results.[3] The discussed mechanism of PS is an alternative to the usual explanation of PS in cuprates, which is attributed to strong antiferromagnetic correlations (see, e.g., Refs. 1 and 2) or nearest-neighbor Coulomb repulsion.[12,15–20] In our approach, the relation between the number of charge carriers and doping level is indirect, which also implies the indirect dependence of T_c versus doping. Using, only for illustration purposes, the simplest BCS expression for T_c, accounting for Coulomb repulsion, we show that $T_c(n)$ is near its maximum within the doping range where PS occurs.

ACKNOWLEDGMENTS

We acknowledge stimulating discussions with A.V. Rozhkov and partial support from the National Security Agency (NSA), Laboratory Physical Sciences (LPS), Army Research Office (ARO), National Science Foundation (NSF) Grant No. EIA-0130383, Russian Foundation for Basic Research (RFBR) (Grants No. 06-02-16691 and No. 08-02-00212), and Core-to-Core program supported by Japan Society for Promotion of Science (JSPS), JSPS-RFBR 06-02-91200, and EU project CoMePhS. S.S. acknowledges support from the Ministry of Science, Culture and Sport of Japan via the Grant-in Aid No. 18740224, EPSRC via Grants EP/D072581/1 and EP/F005482/1, and ESF network-program "Arrays of Quantum Dots and Josephson Junctions."

[1] E. Dagotto, Science **309**, 257 (2005).
[2] E. Nagaev, *Colossal Magnetoresistance and Phase Separation in Magnetic Semiconductors* (Imperial College, London, 2002).
[3] K. M. Lang, V. Madhavan, J. E. Hoffman, E. W. Hudson, H. Eisaki, S. Uchida, and J. C. Davis, Nature (London) **415**, 412 (2002).
[4] J. E. Hoffman, E. W. Hudson, K. M. Lang, V. Madhavan, H. Eisaki, S. Uchida, and J. C. Davis, Science **295**, 466 (2002).
[5] M. Vershinin, S. Misra, S. Ono, Y. Abe, Y. Ando, and A. Yazdani, Science **303**, 1995 (2004).
[6] L. P. Gor'kov and A. V. Sokol, JETP Lett. **48**, 547 (1987).
[7] J. Zaanen and O. Gunnarsson, Phys. Rev. B **40**, 7391 (1989).
[8] V. J. Emery, S. A. Kivelson, and H. Q. Lin, Phys. Rev. Lett. **64**, 475 (1990).
[9] K. Machida, Physica C **158**, 192 (1989); M. Kato, K. Machida, H. Nakanishi, and M. Fujita, J. Phys. Soc. Jpn. **59**, 1047 (1990).
[10] C. S. Hellberg and E. Manousakis, Phys. Rev. Lett. **78**, 4609 (1997); C. T. Shih, Y. C. Chen, and T. K. Lee, Phys. Rev. B **57**, 627 (1998); T. H. Gimm and S. H. Suck Salk, *ibid.* **62**, 13930 (2000); W. O. Putikka and M. U. Luchini, *ibid.* **62**, 1684 (2000).
[11] A. Macridin, M. Jarrell, and Th. Maier, Phys. Rev. B **74**, 085104 (2006).
[12] F. Bucci, C. Castellani, C. Di Castro, and M. Grilli, Phys. Rev. B **52**, 6880 (1995); G. Seibold, C. Castellani, C. Di Castro, and M. Grilli, *ibid.* **58**, 13506 (1998).
[13] W.-F. Tsai and S. A. Kivelson, Phys. Rev. B **73**, 214510 (2006).
[14] M. Grilli, B. G. Kotliar, and A. J. Millis, Phys. Rev. B **42**, 329 (1990).
[15] M. Grilli, R. Raimondi, C. Castellani, C. Di Castro, and G. Kotliar, Phys. Rev. Lett. **67**, 259 (1991).
[16] L. F. Feiner, M. Grilli, and C. Di Castro, Phys. Rev. B **45**, 10647 (1992).
[17] Y. Bang, G. Kotliar, R. Raimondi, C. Castellani, and M. Grilli, Phys. Rev. B **47**, 3323 (1993).
[18] R. Raimondi, C. Castellani, M. Grilli, Y. Bang, and G. Kotliar, Phys. Rev. B **47**, 3331 (1993).
[19] N. Kothekar, K. F. Quader, and D. W. Allender, Phys. Rev. B **51**, 5899 (1995).
[20] M. E. Simon and A. A. Aligia, Phys. Rev. B **53**, 15327 (1996).
[21] L. F. Feiner, J. H. Jefferson, and R. Raimondi, Phys. Rev. Lett. **76**, 4939 (1996).
[22] *The Physics of Superconductors*, edited by K. H. Benneman and J. B. Ketterson (Springer, Berlin, 2004), Vol. II.
[23] K. I. Kugel, A. L. Rakhmanov, and A. O. Sboychakov, Phys. Rev. Lett. **95**, 267210 (2005); A. O. Sboychakov, K. I. Kugel, and A. L. Rakhmanov, Phys. Rev. B **74**, 014401 (2006).
[24] A. Bianconi, G. Bianconi, S. Caprara, D. Di Castro, H. Oyanagi, and N. L. Saini, J. Phys.: Condens. Matter **12**, 10655 (2000).
[25] M. Fratini, N. Poccia, and A. Bianconi, J. Phys.: Conf. Ser. **108**, 012036 (2008).
[26] E. G. Maksimov, Usp. Fiz. Nauk **174**, 1026 (2004) [Phys. Usp. **47**, 957 (2004)].
[27] A. O. Sboychakov, K. I. Kugel, and A. L. Rakhmanov, Phys. Rev. B **76**, 195113 (2007).
[28] L. P. Gor'kov and G. B. Teitel'baum, Phys. Rev. Lett. **97**, 247003 (2006).
[29] E. G. Maksimov and O. V. Dolgov, Usp. Fiz. Nauk **177**, 983 (2007) [Phys. Usp. **50**, 933 (2007)].
[30] V. J. Emery, Phys. Rev. Lett. **58**, 2794 (1987); F. C. Zhang and T. M. Rice, Phys. Rev. B **37**, 3759 (1988).
[31] J. B. Goodenough, Europhys. Lett. **57**, 550 (2002).
[32] L. Hozoi, S. Nishimoto, and A. Yamasaki, Phys. Rev. B **72**, 144510 (2005); L. Hozoi and S. Nishimoto, *ibid.* **73**, 245101 (2006).
[33] A nonzero average $\langle a_\alpha^\dagger a_{\bar{\alpha}} \rangle$ is a well-known internal inconsistency of the Hubbard I approximation at $t_{ab} \neq 0$ (see, e.g., Ref. 37) since it produces a non-Hermitian behavior of the Green functions. However, for the parameter range discussed here, these values are small compared to the coefficients g_α that characterize the maximum band filling in our model, $|\langle a_\alpha^\dagger a_{\bar{\alpha}} \rangle|^2 \ll g_\alpha g_{\bar{\alpha}}$. It can be shown that under the latter condition the effect of $\langle a_\alpha^\dagger a_{\bar{\alpha}} \rangle$ on the band structure and band filling is negligible.
[34] See, e.g., P. Fulde, *Electron Correlations in Molecules and Solids* (Springer-Verlag, Berlin, 1991); S. G. Ovchinnikov and V. V. Val'kov, *Hubbard Operators in the Theory of Strongly*

Correlated Electrons (Imperial College, London, 2004).
[35] J. Mizia and G. Górski, *Models of Itinerant Ordering in Crystals* (Elsevier, Amsterdam, 2007).
[36] D. M. Newns, P. C. Pattnaik, and C. C. Tsuei, Phys. Rev. B **43**, 3075 (1991).
[37] J. Hubbard, Proc. R. Soc. London **A281**, 401 (1964).
[38] P. G. de Gennes, *Superconductivity of Metals and Alloys* (Perseus Books, New York, 1999).
[39] E. Dagotto, A. Nazarenko, and A. Moreo, Phys. Rev. Lett. **74**, 310 (1995).